

SUPPLEMENTARY INFORMATION

Surface charge and particle size determine the metabolic fate of dendritic polyglycerols

Kritee Pant[†], Johanna Pufe[†], Kristof Zarschler[†], Ralf Bergmann[†], Jörg Steinbach^{†,§}, Sabine Reimann[‡], Rainer Haag^{‡,}, Jens Pietzsch^{†,§,*}, and Holger Stephan^{†,*}*

[†]Helmholtz-Zentrum Dresden - Rossendorf, Institute of Radiopharmaceutical Cancer Research, Bautzner Landstrasse 400, D-01328 Dresden, Germany.

[‡]Organische Chemie, Institut für Chemie und Biochemie, Freie Universität Berlin, Takustrasse 3, D-14195, Berlin, Germany.

[§]Technische Universität Dresden, Department of Chemistry and Food Chemistry, D-01062 Dresden, Germany.

Corresponding author

Dr. Holger Stephan, Helmholtz-Zentrum Dresden - Rossendorf, Institute of Radiopharmaceutical Cancer Research, Bautzner Landstrasse 400, 01328 Dresden, Germany, Phone: +49 3512603091, Fax: +49 3512603232, E-Mail: h.stephan@hzdr.de

Prof. Dr. Jens Pietzsch, Helmholtz-Zentrum Dresden - Rossendorf, Institute of Radiopharmaceutical Cancer Research, Bautzner Landstrasse 400, 01328 Dresden, Germany, Phone: +49 3512602622, Fax: +49 3512603232, E-Mail: j.pietzsch@hzdr.de

Prof. Dr. Rainer Haag, Freie Universität Berlin, Institut für Chemie und Biochemie, Organische Chemie, Takustrasse 3, 14195, Berlin, Germany, Phone: +49 30 83852633, Fax: +49 30 8384 52633, E-Mail: haag@chemie.fu-berlin.de

Corresponding email: h.stephan@hzdr.de

Table of Contents:

Table S1	Characteristics of dPG and dPGS derivatives
Figure S1	$^1\text{H-NMR}$ of dPG-NOTA 130 kDa in D_2O
Figure S2	Analytical RP-HPLC chromatogram of 3
Figure S3	Radiometric titration of dPG-NOTA and dPGS-NOTA conjugates with ^{68}Ga to determine chelator/polymer ratio
Figure S4	Illustration of dPG and dPGS azide conjugates with Rhodamine B derivative
Figure S5	Cell viability determination of Ga-loaded dPG-/dPGS-NOTA conjugates
Table S2	Specific radioactivity of ^{68}Ga-labeled dPG-NOTA and dPGS-NOTA conjugates
Figure S6	Radiochemical analysis via radio-TLC and size exclusion chromatography
Figure S7	Blocking studies with THP-1 macrophages cell line
Figure S8	Radio-stability experiments against apo-transferrin using SDS-PAGE
Figure S9	Protein interactions with fibrinogen and apo-transferrin using MST
Figure S10	Whole body distribution of [^{68}Ga]Ga-dPG-/dPGS-NOTA conjugates represented in SUV
Table S3	Percentage of activity accumulation in bone (femur)
Table S4	Quantitative evaluation (values) of the radiolabeled [^{68}Ga]Ga-dPG-NOTA (7-9) conjugates (%ID/g)
Table S5	Quantitative evaluation (values) of the radiolabeled [^{68}Ga]Ga-dPGS-NOTA (10-12) conjugates (%ID/g)
Figure S11	Representative maximum intensity projections (MIP) of the PET-studies with [^{68}Ga] Ga-9 (A, B, C) and [^{68}Ga] Ga-12
Figure S12	Biokinetics of [^{68}Ga]Ga-dPG-NOTA (9) as well as of [^{68}Ga]Ga-dPGS-NOTA (12) with and without blocking agents
Table S6	Half-lives of the [^{68}Ga]Ga-dPG-NOTA (9) and [^{68}Ga]Ga-dPGS-NOTA (12) in the blood without (control)
Table S12	Hydrodynamic diameter measurement of dPG-/dPGS-NOTA in different pH using DLS

Table S1 Characteristics of dPG and dPGS derivatives. Number of amine groups was calculated via ^1H NMR of the precursor. The hydrodynamic diameter (distribution by number) and ζ -potential measurements were performed by dynamic light scattering in 10 mM phosphate buffer at pH 7.4. The values given are from three independent measurements. All samples were sonicated for 5 min prior to the experiments.

Polymer NP	M_w (g mol^{-1})	No. of amines	$d_h \pm SD^e$ (nm)	ζ -potential \pm SD^e (mV)	PDI
1	4500	4-5	3.8 ± 0.8	$+1.5 \pm 2.0$	0.48
2	10000	13-14	4.6 ± 0.2	$+4.6 \pm 1.8$	0.38
3	130000	138-140	8.1 ± 0.8	$+9.3 \pm 1.2$	0.36
4	10000	4-5	4.8 ± 1.0	-19.6 ± 2.8	0.44
5	22300	13-14	6.5 ± 1.5	-26.8 ± 3.5	0.40
6	290000	138-140	9.0 ± 0.5	-34.0 ± 2.0	0.45

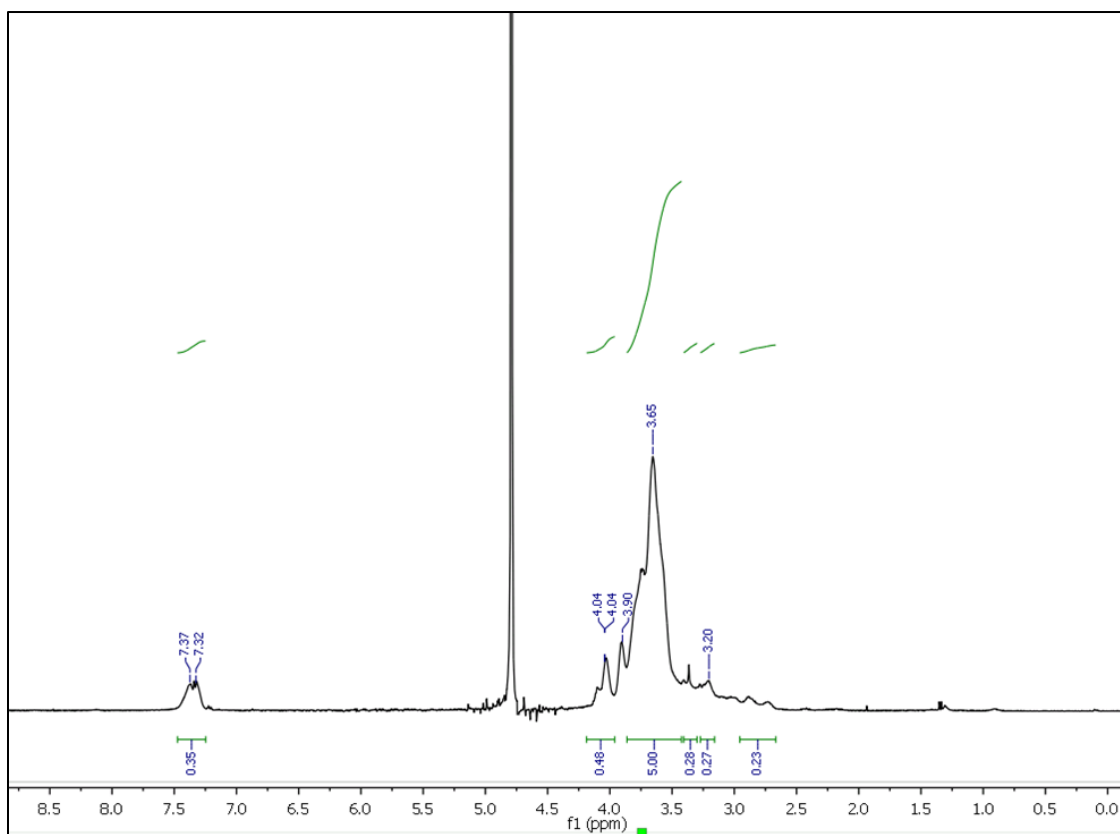


Figure S1 ^1H -NMR of dPG-NOTA 130 kDa as an example. Analysis of conjugation of NOTA to the amine terminated dPG was done also using ^1H -NMR in D_2O (400 MHz)

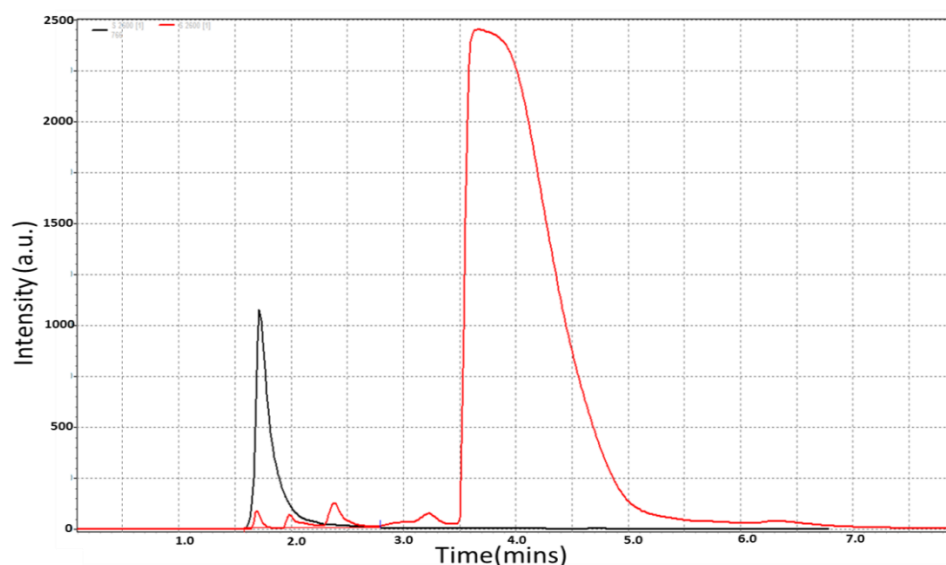


Figure S2 Analytical RP-HPLC chromatogram of dPG-NOTA-130 kDa (**3**) (*black*; $t_R = 1.7 \text{ min}$) and *p*-SCN-Bn-NOTA (*red*; $t_R = 3.6 \text{ min}$) using a Phenomenex RP18 in an isocratic run of 55:45 with ACN (0.1% TFA) and water (0.1% TFA) at a flow rate of 1 mL min^{-1} .

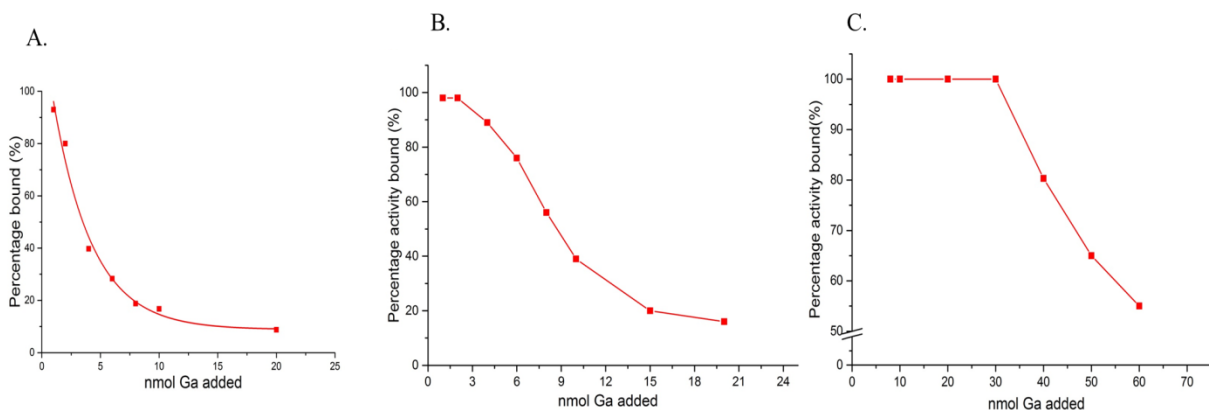


Figure S3 Plot of percentage of $[^{68}\text{Ga}]\text{GaCl}_3$ specifically bound (*y-axis*) vs. nanomoles of gallium added (*x-axis*) A. **7**, B. **8** and C. **9**, as determined by radio-thin layer chromatography analysis.

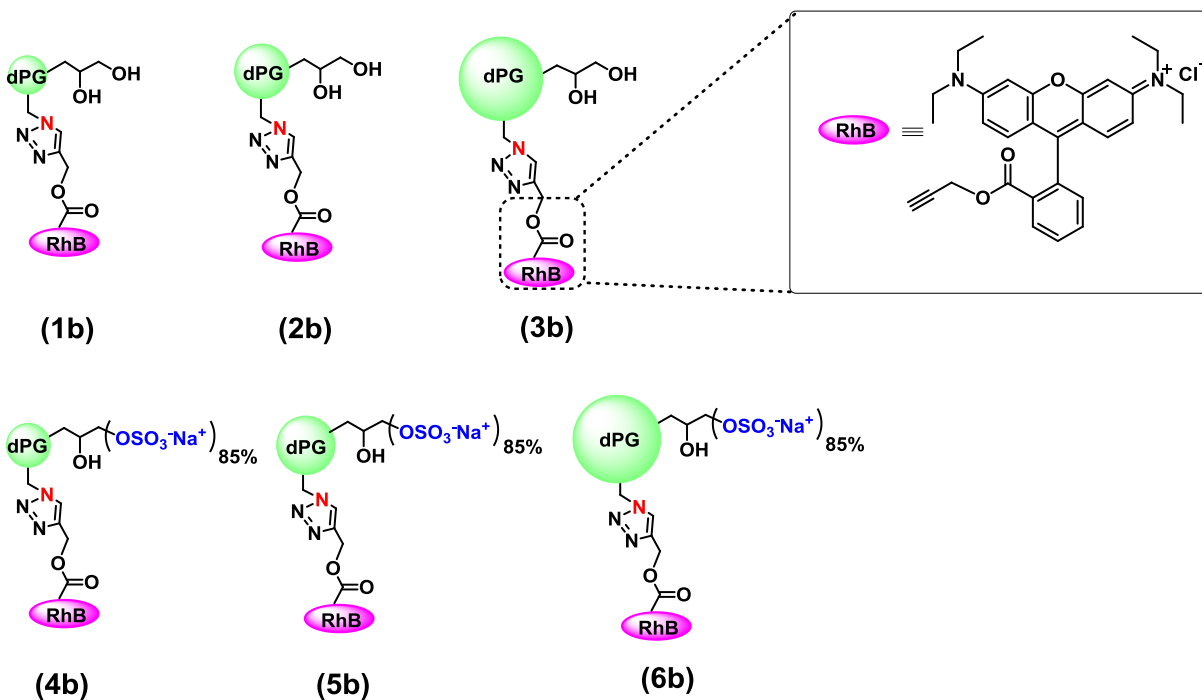


Figure S4 Synthesis and conjugation of different size and charge azide terminated dPG and dPGS with derivatized alkyne-containing Rhodamine B derivative. Inset: chemical structure of Rhodamine B derivative.

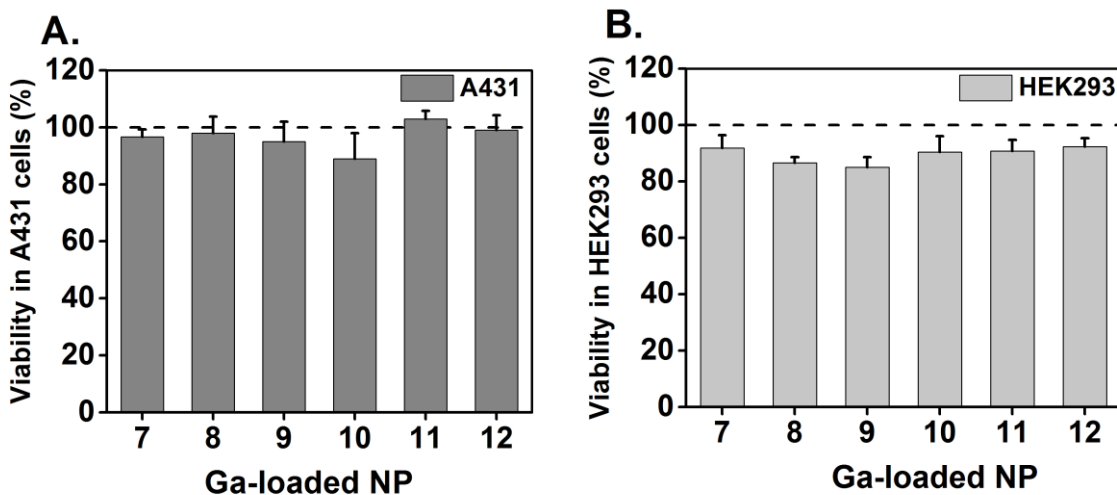


Figure S5 Cell Viability determination. Determination of the cellular viability of Ga-loaded dPG-/dPGS-NOTA conjugates (7-12) after 72 h in A431 cells and HEK293 cells with the concentration of $500 \mu\text{g mL}^{-1}$ (highest concentration used) using the MTS assay. Triton™ X-100 was used as a positive control and untreated cells were taken as the negative control. The percentage of cell viability is expressed relative to the negative control.

Table S2 Radiochemical purity and specific activity of the [⁶⁸Ga]Ga-dPG-/dPGS-NOTA conjugates.

⁶⁸ Ga-Conjugate	Radiochemical Purity (after SEC)	Specific Activity (MBq/μg)
[⁶⁸ Ga]Ga-7	≥ 98.0%	0.20 MBq/μg
[⁶⁸ Ga]Ga-8	≥ 98.5%	0.31 MBq/μg
[⁶⁸ Ga]Ga-9	≥ 99.1%	0.36 MBq/μg
[⁶⁸ Ga]Ga-10	≥ 99.0%	0.19 MBq/μg
[⁶⁸ Ga]Ga-11	≥ 98.9%	0.35 MBq/μg
[⁶⁸ Ga]Ga-12	≥ 99.0%	0.36 MBq/μg

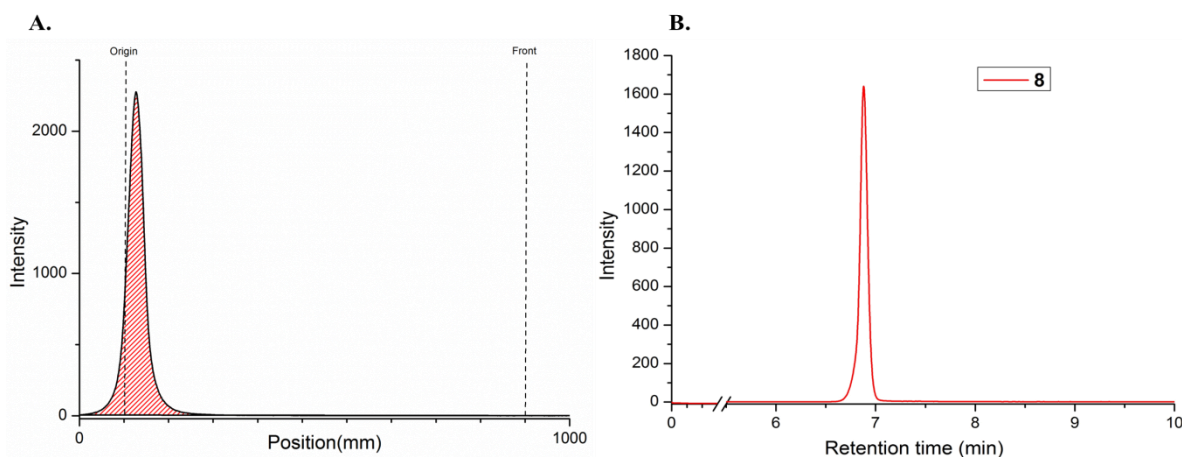


Figure S6 A. Radio-thin layer chromatogram of [⁶⁸Ga]Ga-**8** in 0.1 M citrate buffer pH 5.0. The [⁶⁸Ga]Ga-dPG-/dPGS-NOTA conjugates stay at the origin (start) and the ⁶⁸Ga[Ga] forms a complex with the citrate which runs to the front. **B.** Analytical SEC chromatogram of [⁶⁸Ga]Ga-**8** on a Knauer HPLC system with a self-packed Sephadex G25 column connected to a UV detector as well as a RITA activity detector at 0.8 mL min⁻¹. The characterization of other [⁶⁸Ga]Ga-dPG-/dPGS-NOTA conjugates (**7-12**) was done using the same protocol.

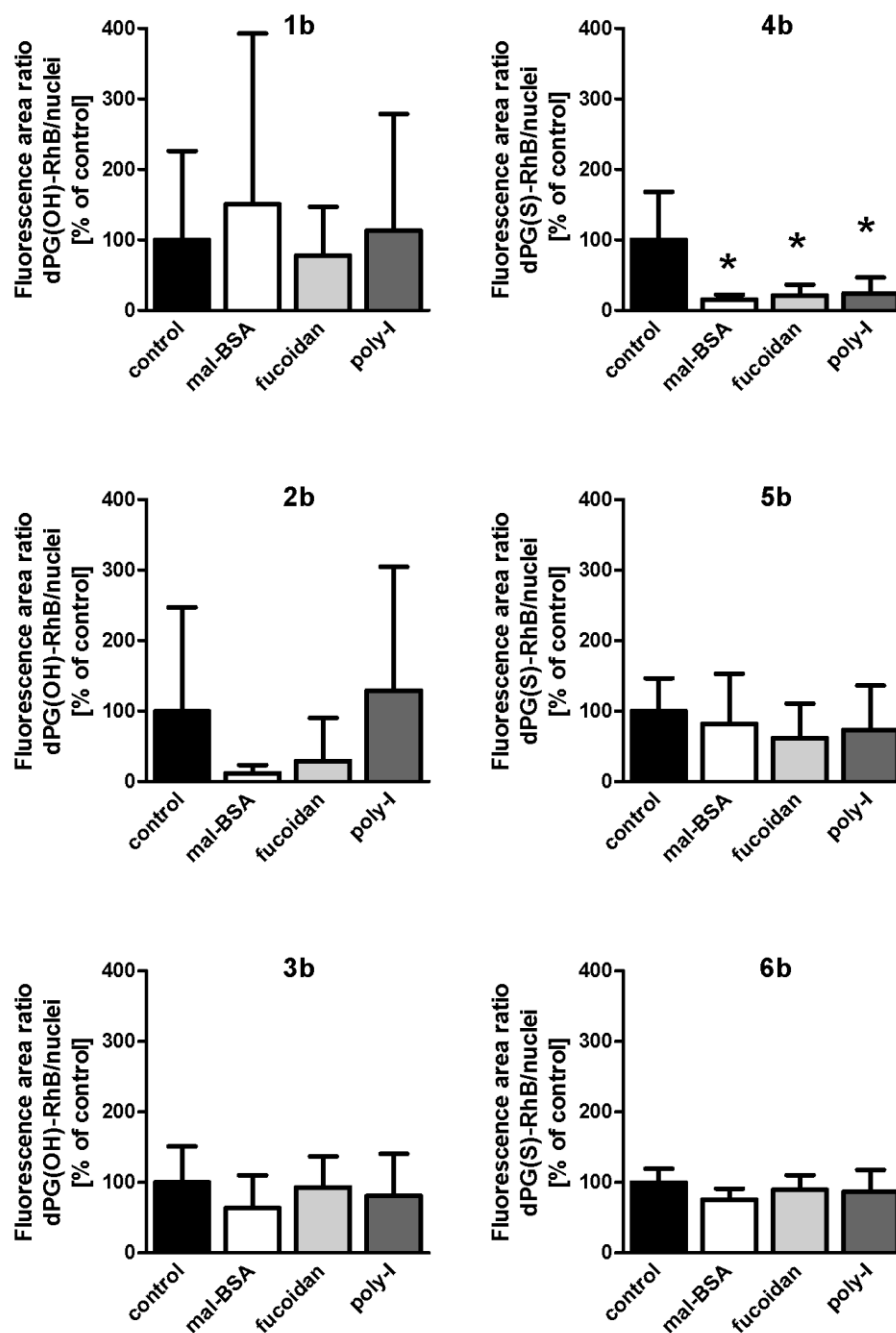


Figure S7 Blocking of SR mediated uptake of **1b-6b** particles in THP-1 M ϕ . Graphs show the area ratio of RhB fluorescence (NP) to nuclei fluorescence of THP-1 M ϕ , preincubated without (control) or with mal-BSA (36 μ M), fucoidan (65.5 μ g mL⁻¹) or poly-I (60 μ g mL⁻¹) before exposed to 2 μ M **1b-6b**. Values are given in percent of the control (100%) and represent mean + SEM from four different images of three independent experiments (nonparametric Kruskal-Wallis test with Dunn's post-test for significance ($p < 0.05$, $n = 12$)).

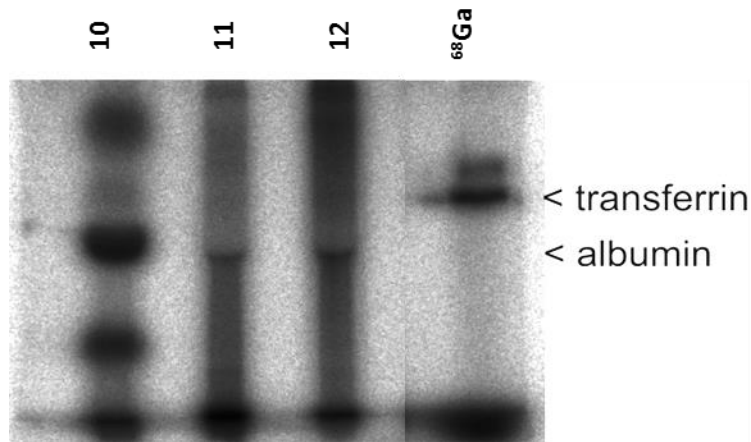


Figure S8 Native PAGE to determine transchelation of [^{68}Ga]Ga from [^{68}Ga]Ga-dPG-/dPGS-NOTA conjugates to apo-transferrin. Although no dark band could be seen in the transferrin range, a quantitative evaluation was not possible due to smear because of polydispersity.

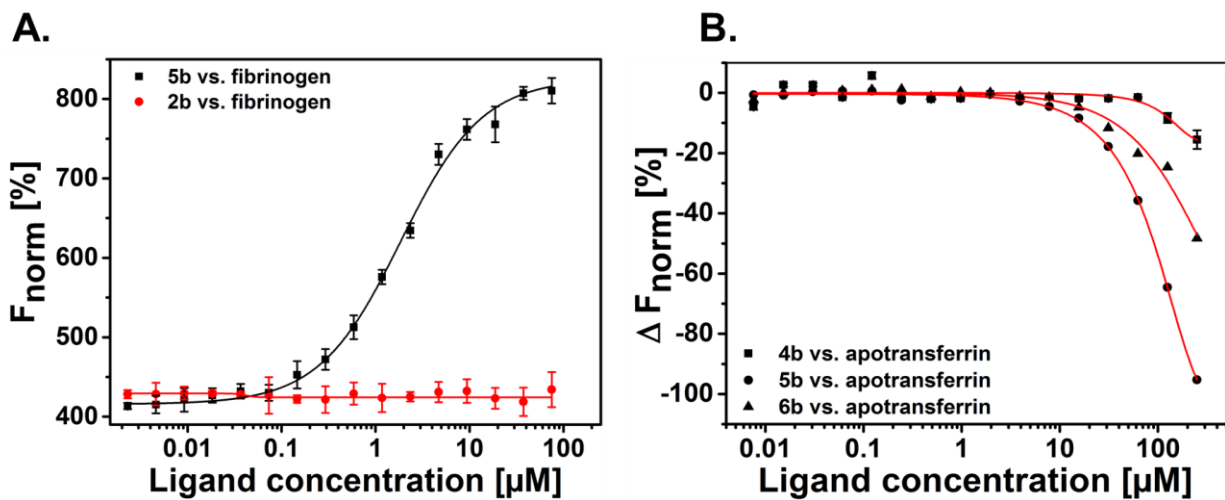


Figure S9 A. MST thermogram of interactions with fibrinogen (75 μM - 0.0023 μM) resulting in a K_d of 1.22 μM . **B.** Comparison of interactions of dPG(S)-RhB conjugates 4b, 5b, and 6b with apo-transferrin.

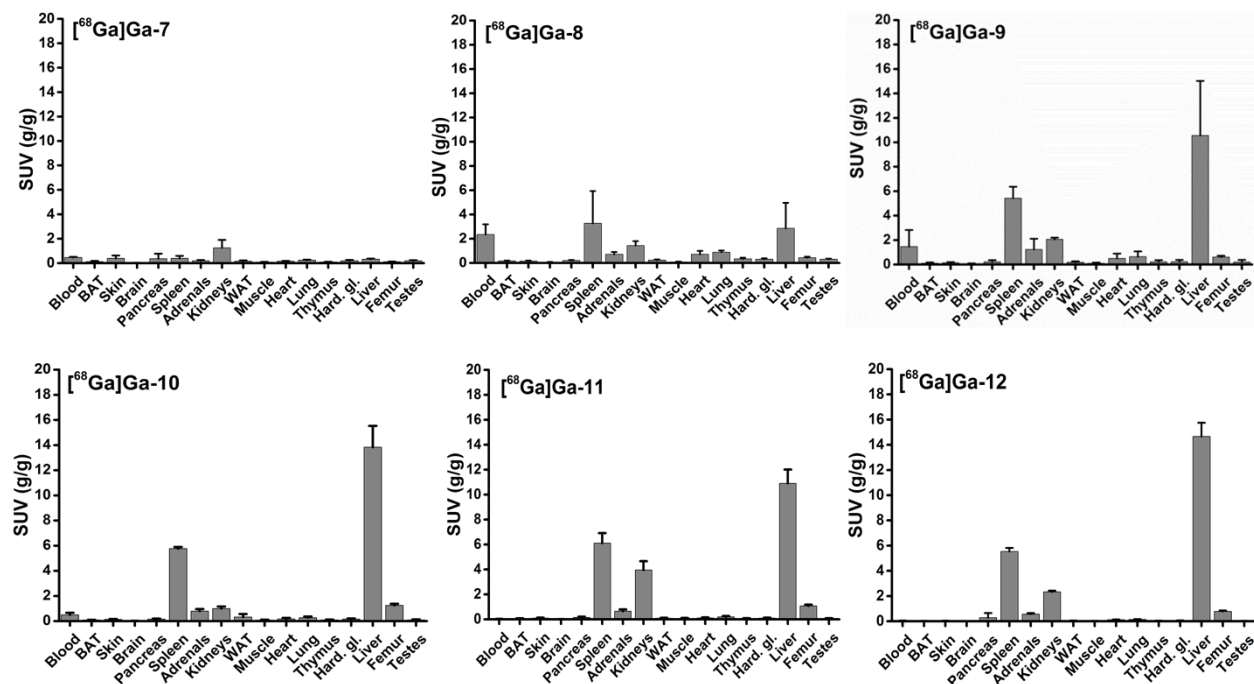


Figure S10 Biodistribution profile of $[^{68}\text{Ga}]\text{Ga}$ -labeled dPG-/dPGS-NOTA conjugates (**7-12**) 1 h post intravenous injection to the tail vein of healthy Wistar rats ($n = 8$, except for **9** and **12** where $n = 4$). The values are denoted in standard uptake values.

Table S3 Accumulation in the bone (femur) of the radiolabeled $[^{68}\text{Ga}]\text{Ga}$ -dPG-/dPGS-NOTA conjugates (**7-12**) after 60 min in healthy Wistar rats ($n = 8$, except for **9** and **12** where $n = 4$). The value is given as standard uptake value.

Compound	Accumulation in Femur (Bone) (standard uptake value (gram per gram))
7	0.12 ± 0.02
8	0.43 ± 0.08
9	0.62 ± 0.08
10	1.24 ± 0.14
11	1.07 ± 0.04
12	0.77 ± 0.08

Table S4 Quantitative evaluation of the radiolabeled [⁶⁸Ga]Ga-dPG-NOTA conjugates in healthy Wistar rats (n = 8, except for **9** where n=4). The value is given as a percentage of the injected dose per gram and percent of injected dose.

Organs (%ID/g ± SD) <i>5 min p.i.</i>	7	8	9
Blood	1.46 ± 0.22	3.75 ± 1.04	4.68 ± 0.35
BAT	0.27 ± 0.06	0.33 ± 0.11	0.27 ± 0.08
Skin	0.44 ± 0.08	0.38 ± 0.10	0.33 ± 0.03
Brain	0.05 ± 0.01	0.11 ± 0.02	0.12 ± 0.00
Pancreas	0.28 ± 0.05	0.38 ± 0.11	0.32 ± 0.07
Spleen	0.31 ± 0.09	2.59 ± 1.98	3.31 ± 0.42
Adrenals	0.68 ± 0.55	1.07 ± 0.44	0.82 ± 0.13
Kidneys	3.56 ± 1.21	3.22 ± 0.65	2.59 ± 0.25
WAT	0.91 ± 1.57	0.80 ± 0.70	0.41 ± 0.17
Muscle	0.28 ± 0.28	0.28 ± 0.19	0.16 ± 0.02
Heart	0.50 ± 0.15	0.91 ± 0.15	1.05 ± 0.29
Lung	0.67 ± 0.11	1.32 ± 0.24	1.36 ± 0.37
Thymus	0.30 ± 0.06	0.49 ± 0.05	0.47 ± 0.07
Harderian gland	0.35 ± 0.06	0.43 ± 0.13	0.45 ± 0.13
Liver	0.56 ± 0.15	2.08 ± 1.20	3.73 ± 0.31
Femur	0.31 ± 0.10	0.55 ± 0.08	0.51 ± 0.04
Testes	0.24 ± 0.09	0.36 ± 0.16	0.22 ± 0.02
Organs (%ID ± SD)			
Intestine	2.43 ± 0.22	3.15 ± 1.48	2.22 ± 0.09
Stomach	0.54 ± 0.12	0.12 ± 0.06	0.34 ± 0.03
Urine	45.44 ± 12.93	13.87 ± 9.19	16.03 ± 2.15

Organs (%ID/g ± SD) <i>60 min p.i.</i>	7	8	9
Blood	0.30 ± 0.04	1.84 ± 0.73	2.05 ± 0.12
BAT	0.08 ± 0.03	0.13 ± 0.02	0.13 ± 0.01
Skin	0.26 ± 0.18	0.13 ± 0.02	0.11 ± 0.03
Brain	0.02 ± 0.01	0.06 ± 0.01	0.07 ± 0.01
Pancreas	0.24 ± 0.28	0.16 ± 0.03	0.22 ± 0.11
Spleen	0.25 ± 0.13	2.60 ± 2.19	4.46 ± 0.51
Adrenals	0.13 ± 0.05	0.56 ± 0.17	1.17 ± 0.80
Kidneys	0.82 ± 0.41	1.12 ± 0.32	1.44 ± 0.07
WAT	0.11 ± 0.05	0.18 ± 0.04	0.13 ± 0.05
Muscle	0.05 ± 0.02	0.07 ± 0.02	0.10 ± 0.05
Heart	0.10 ± 0.01	0.56 ± 0.24	0.65 ± 0.07
Lung	0.16 ± 0.03	0.69 ± 0.14	0.78 ± 0.06
Thymus	0.06 ± 0.01	0.27 ± 0.08	0.26 ± 0.03
Harderian gland	0.12 ± 0.03	0.24 ± 0.05	0.27 ± 0.03
Liver	0.21 ± 0.05	2.26 ± 1.74	4.47 ± 0.32
Femur	0.08 ± 0.02	0.34 ± 0.08	0.42 ± 0.03
Testes	0.13 ± 0.04	0.24 ± 0.05	0.27 ± 0.04
Organs (%ID ± SD)			
Intestine	1.89 ± 0.39	2.76 ± 0.90	4.37 ± 2.07
Stomach	0.16 ± 0.11	0.18 ± 0.03	0.50 ± 0.50
Urine	87.97 ± 25.37	48.51 ± 15.27	22.62 ± 11.65

Table S5 Quantitative evaluation of the radiolabeled [⁶⁸Ga]Ga-dPGS-NOTA conjugates (**10-12**) in healthy Wistar rats (n = 8 except for **12** where n=4). The value is given as a percentage of the injected dose per gram and percent of injected dose.

Organs (%ID/g ± SD) <i>5 min p.i</i>	10	11	12
Blood	1.92 ± 0.73	0.62 ± 0.23	0.29 ± 0.02
BAT	0.33 ± 0.08	0.14 ± 0.07	0.05 ± 0.01
Skin	0.48 ± 0.11	0.23 ± 0.14	0.09 ± 0.01
Brain	0.06 ± 0.03	0.03 ± 0.01	0.01 ± 0.00
Pancreas	0.30 ± 0.06	0.23 ± 0.04	0.14 ± 0.02
Spleen	4.75 ± 2.17	5.32 ± 2.02	7.58 ± 0.72
Adrenals	1.25 ± 0.36	0.97 ± 0.33	0.86 ± 0.23
Kidneys	2.74 ± 1.07	3.70 ± 0.67	2.25 ± 0.06
WAT	0.93 ± 0.70	0.34 ± 0.33	0.12 ± 0.07
Muscle	0.28 ± 0.14	0.10 ± 0.06	0.04 ± 0.01
Heart	0.56 ± 0.18	0.24 ± 0.06	0.17 ± 0.03
Lung	0.93 ± 0.26	0.38 ± 0.10	0.29 ± 0.01
Thymus	0.43 ± 0.16	0.16 ± 0.07	0.08 ± 0.01
Harderian gland	0.93 ± 1.35	0.19 ± 0.09	0.07 ± 0.01
Liver	17.85 ± 3.01	9.55 ± 0.50	17.52 ± 1.15
Femur	0.92 ± 0.36	0.87 ± 0.27	1.00 ± 0.04
Testes	0.20 ± 0.03	0.13 ± 0.06	0.06 ± 0.01
Organs (%ID ± SD)			
Intestine	1.36 ± 0.15	0.79 ± 0.06	0.53 ± 0.10
Stomach	0.46 ± 0.01	0.30 ± 0.15	0.07 ± 0.02
Urine	4.88 ± 1.43	2.81 ± 0.66	0.85 ± 0.35

Organs (%ID/g ± SD) <i>60 min p.i</i>	10	11	12
Blood	0.38 ± 0.25	0.06 ± 0.04	0.06 ± 0.01
BAT	0.09 ± 0.02	0.05 ± 0.01	0.03 ± 0.01
Skin	0.13 ± 0.03	0.08 ± 0.02	0.05 ± 0.01
Brain	0.02 ± 0.01	0.01 ± 0.00	0.01 ± 0.00
Pancreas	0.15 ± 0.05	0.13 ± 0.05	0.32 ± 0.39
Spleen	5.34 ± 1.72	4.33 ± 1.32	6.39 ± 0.57
Adrenals	0.79 ± 0.22	0.53 ± 0.16	0.64 ± 0.06
Kidneys	0.96 ± 0.16	3.21 ± 0.92	2.69 ± 0.26
WAT	0.33 ± 0.29	0.07 ± 0.03	0.04 ± 0.02
Muscle	0.08 ± 0.05	0.05 ± 0.03	0.03 ± 0.01
Heart	0.18 ± 0.14	0.09 ± 0.04	0.14 ± 0.04
Lung	0.27 ± 0.16	0.16 ± 0.07	0.16 ± 0.04
Thymus	0.09 ± 0.06	0.06 ± 0.01	0.05 ± 0.01
Harderian gland	0.16 ± 0.08	0.08 ± 0.02	0.07 ± 0.02
Liver	17.48 ± 2.16	9.92 ± 1.19	16.94 ± 2.02
Femur	0.90 ± 0.58	0.71 ± 0.27	0.89 ± 0.09
Testes	0.11 ± 0.06	0.06 ± 0.01	0.04 ± 0.00
Organs (%ID ± SD)			
Intestine	1.16 ± 0.07	0.97 ± 0.34	0.33 ± 0.22
Stomach	0.18 ± 0.04	0.19 ± 0.14	0.08 ± 0.02
Urine	4.77 ± 4.73	4.98 ± 1.51	4.23 ± 1.42

Blocking studies using competitive inhibitors

To further examine the physiological fate of the polyglycerols, blocking studies were also conducted. In this regard, competitive blocking studies were performed with [^{68}Ga]Ga-**9** and [^{68}Ga]Ga-**12** using the unlabeled counterparts in excess of 31 nmol kg^{-1} . Furthermore, as the higher molecular weight polyglycerols exhibited an inherent phagocytic avidity *in vitro*, mal-BSA (60 nmol/kg body weight), a scavenger receptor blocking agent was also used to compare if increased blocking of the binding sites impacts on the biodistribution and pharmacokinetics profile.

To test the interaction of the largest neutral dPG-NOTA conjugate (**9**) and anionic (**12**) dPGS-NOTA conjugates with the liver, spleen and kidneys, their non-radiolabeled counterparts or mal-BSA were simultaneously injected. The liver uptake of the both the conjugates [^{68}Ga]Ga-**9** and [^{68}Ga]Ga-**12** decreased with the simultaneous injection with their non-radiolabeled counterparts (**SI Figure 12**). In general, this behavior could be ascribed to the competition of the nanoparticles for the binding sites in the liver. The blocking effect of the pan SR ligand mal-BSA *in vivo*, in contrast, was not very pronounced. Only for [^{68}Ga]Ga-**12** a substantial mal-BSA-mediated blocking of liver accumulation could be observed. Both the blocking agents increased the accumulation of the radiolabeled dPG-/dPGS-NOTA conjugates in the spleen. In the kidneys, the distribution of the [^{68}Ga]Ga-**9** was reduced by both the blocking agents. On the other hand, both the blocking inhibitors increased the distribution of the anionic [^{68}Ga]Ga-**12**. The increasing accumulation in the spleen and the kidneys could be attributed to the desorption of the [^{68}Ga]Ga-dPG-/dPGS-NOTA conjugates in the circulation from the low affine binding sites which results in a transient increase in the organ accumulation. Regarding the use of mal-BSA, the observed effects can be ascribed to a partly blocking of SR-A, and other SR, in the liver. This, in consequence, is expected to reroute particles to other organs. This could be clearly observed for **12** but not for **9**. One explanation could be the overall low affinity of mal-BSA to SR-A, in comparison to varying affinities of the different particles and, on the other hand, the low blocking concentration of the mal-BSA tolerated in rats. This pilot investigation, therefore, only marginally strengthens our hypothesis.

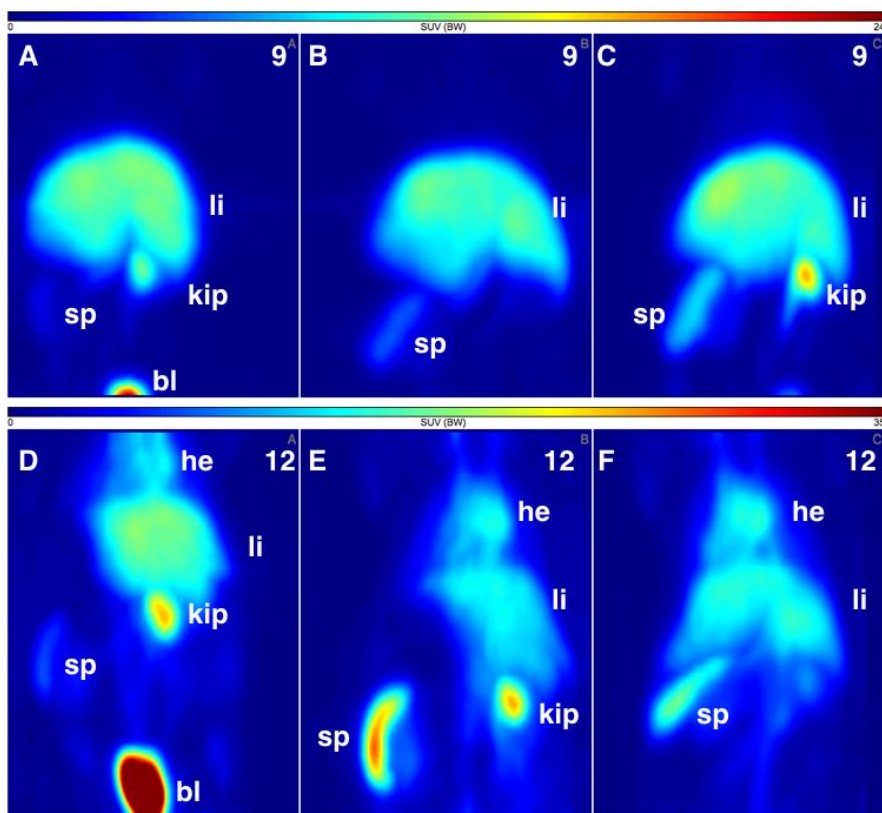


Figure S11 Representative maximum intensity projections (MIP) of the PET-studies with [^{68}Ga]Ga-**9** (A,B,C) and [^{68}Ga]Ga-**12** (D,E,F) at 90 min post injection without (A,D) and with simultaneous injection of the non-radiolabeled counterparts (B,E) and mal-BSA (C,F); heart (he), liver (li), (kip) kidney pelvis, (sp) spleen, (bl) bladder.

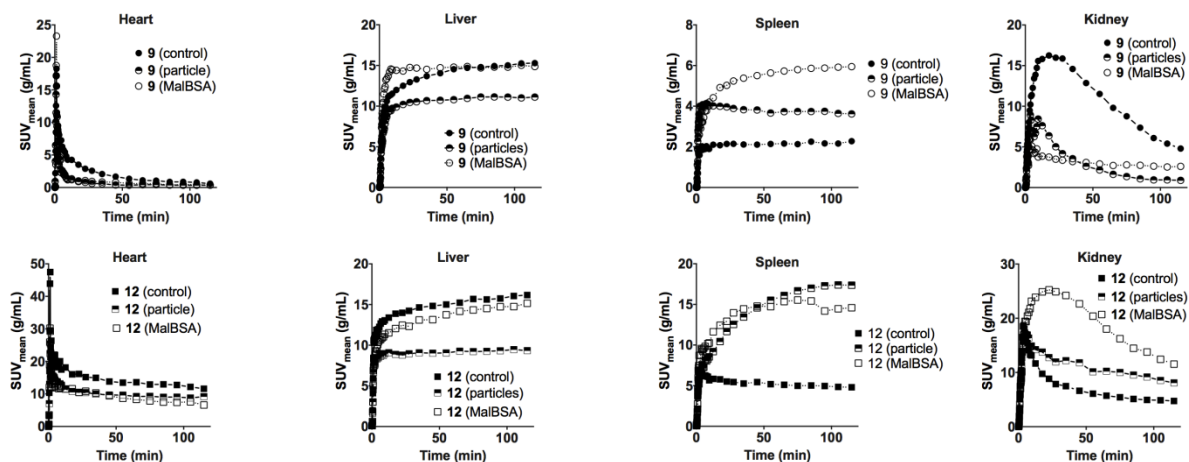


Figure S12 Biokinetics of [^{68}Ga]Ga-dPG-NOTA (**9**) as well as of [^{68}Ga]Ga-dPGS-NOTA (**12**) in the heart, liver, spleen and kidney measured with PET after single intravenous injection. The time-activity concentration curves were derived from the corresponding ROIs and were calculated as SUV_{mean} (g/mL). The blocking was achieved by simultaneous injection of 31 nmol/kg body weight of the non-radiolabeled counterpart of the dPGs (particle) and mal-BSA (60 nmol/kg body weight).

Table S6 Half-life of the [^{68}Ga]Ga-dPG-NOTA (**9**) and [^{68}Ga]Ga-dPGS-NOTA (**12**) in the blood without (control) and with simultaneous injection of 31 nmol/kg body weight of the non-radiolabeled counterpart of the particles and 60 nmol/kg body weight mal-BSA.

Conjugates	9	9	9	12	12	12
	(Control)	(particles)	(mal-BSA)	(Control)	(particles)	(mal-BSA)
Half-life	14.1	9.6	18.2	35.9	19.1	24.7
95% confidence interval	8.4 to 26.3	7.7 to 12.2	16.3 to 20.3	27.9 to 49.2	13.4 to 29.1	19.33 to 33.3

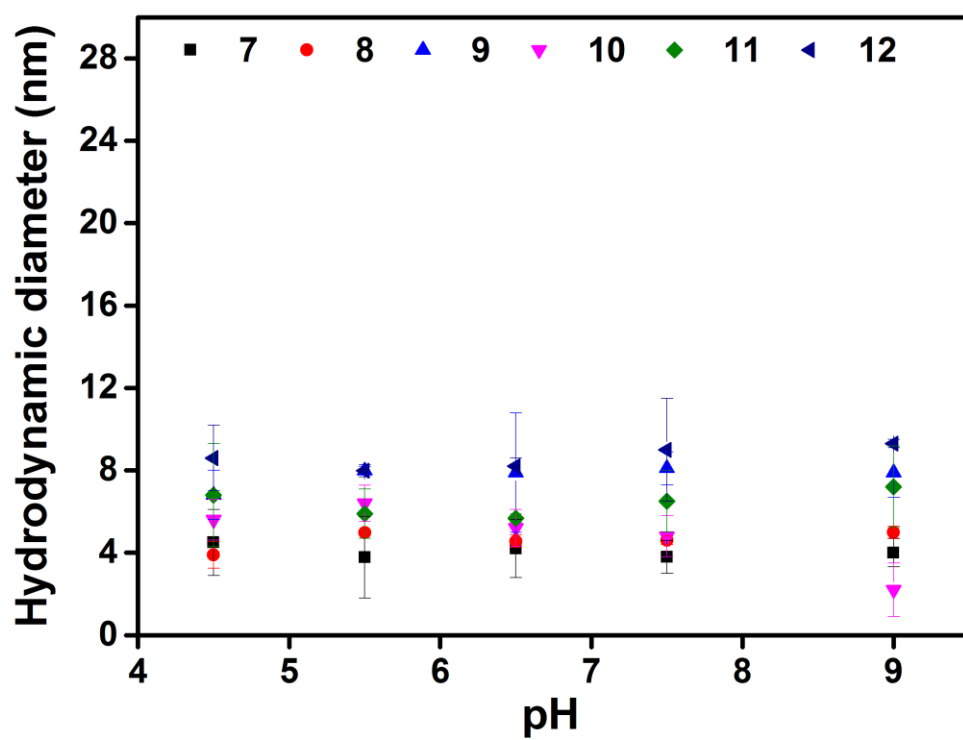


Figure S12 DLS measurement of dPG-/dPGS-NOTA conjugates. Hydrodynamic diameter of dPG-/dPGS-NOTA conjugates at different pH.